Current Applied Physics 11 (2011) 525–531

Contents lists available at ScienceDirect

Current Applied Physics

journal homepage: www.elsevier.com/locate/cap

Effect of In, Sb and Ga doping on the structure and vibrational modes of hydrothermally grown ZnO nanostructures

A. Escobedo-Morales [a,b], U. Pal [b,*]

[a] Facultad de Ingeniería Química, Benemérita Universidad Autónoma de Puebla, C.P. 72570, Puebla, Pue., Mexico
[b] Instituto de Física, Benemérita Universidad Autónoma de Puebla, Apdo. Postal J-48, C.P. 72570, Puebla, Pue., Mexico

ARTICLE INFO

Article history:
Received 1 April 2010
Accepted 7 September 2010
Available online 17 September 2010

Keywords:
Nanostructures
Zinc oxide
Doping
Phonon modes

ABSTRACT

Effect of common optoelectronic dopants like In, Sb and Ga on the structure, morphology and vibrational modes of ZnO nanostructures has been studied systematically using scanning electron microscopy (SEM), X-ray diffraction (XRD), and Raman spectroscopy. While incorporation of Ga has no strong effect on the lattice parameters and crystallinity of ZnO nanostructures, In and Sb doping introduce considerable lattice distortion. Sb doping results an anisotropic distortion along the *c* axis of the ZnO unit cell. Several anomalous vibrational modes are induced due to incorporation of dopants into ZnO lattice. Origins of the observed anomalous modes are discussed.

1. Introduction

ZnO is one of the most promising semiconductors in optoelectronics. Its wide direct band gap (3.37 eV at 300 K) and large exciton binding energy (60 meV) make it an excellent candidate for applications such as light emitting diode [1], laser [2], field emission device [3], chemical sensor [4], and catalyst [5]. In nanostructure form, ZnO promises to increase the efficiency of such applications. As morphology and chemical composition of semiconductor nanostructures affect their optoelectronic properties, a vast effort has been devoted to synthesize ZnO nanostructures of various morphologies through chemical [6–8] and physical [9–11] processes, along with attempts to control their chemical composition through doping process during the last few years [12–14].

Since, it is important to understand how the dopants influence the physical and optoelectronic properties of ZnO nanostructures prior to their practical applications, effect of metal doping on the structure and vibrational properties of ZnO nanostructures has also been studied [15–17]. It has been observed that metal doping severely affects the vibrational characteristics of ZnO nanostructures. For example, broadening and intensity reduction of first-order Raman peaks have been reported in doped ZnO nanostructures [18,19]. Furthermore, the doping process frequently results the appearance of additional Raman peaks, most of which are attributed to local vibrational modes (LVM's) [20–22]. However, the origin of such anomalous Raman modes in metal doped ZnO nanostructures remains controversial [23–25].

In the present article, we have studied the effect of metal doping at different concentrations, on the structure and vibrational properties of ZnO nanostructures systematically. The doped and undoped ZnO nanostructures are characterized by scanning electron microscopy (SEM), X-ray diffraction (XRD), and Raman spectroscopy technique. Possible origins of the observed additional phononic modes are discussed.

2. Experimental section

The doped and undoped ZnO nanostructures used in this study were grown in powder form through a low temperature hydrothermal process, as has been reported earlier [26–28]. Different nominal concentrations (0.5, 1.0 and 2.0 mol%) of indium, antimony or gallium were incorporated into the ZnO nanostructures during their synthesis. While 90 °C was used as synthesis temperature for growing indium doped samples, 110 °C was selected to grow antimony and gallium doped samples in order to increase the solubility of doping precursors (salts) in the reaction media. It has been observed that while the incorporated indium and antimony remain partially segregated in minority phases [26,27], gallium incorporates successfully into the lattice of the ZnO nanostructures through hydrothermal process [28]. The minority phases, identified as indium hydroxide [$In(OH)_3$] and two allotropes of antimony oxide (Sb_2O_3) in as-grown nanostructures could be successfully dissociated by adequate annealing process in inert atmosphere

* Corresponding author. Tel.: +52 222 2295500; fax: +52 222 2295611.
E-mail address: upal@sirio.ifuap.buap.mx (U. Pal).

1567-1739/$ – see front matter © 2010 Elsevier B.V. All rights reserved.
doi:10.1016/j.cap.2010.09.007

[26,27]. The annealing temperatures were chosen close or slightly higher than the melting point of the minority phases to dissociate them and to promote their incorporation into the ZnO lattice. 300 °C and 500 °C were used as annealing temperatures to dissociate the $In(OH)_3$ and Sb_2O_3 phases, respectively. Since antimony and gallium doped samples were grown under similar conditions, for comparison, 500 °C was also set as annealing temperature for the gallium doped samples.

All the samples were analyzed by scanning electron microscopy (Jeol JSM 5300), X-ray diffraction (XRD) (Phillips X'Pert diffractometer, CuKα, 1.5406 Å) and room temperature Raman spectroscopy in backscattering configuration using the 633 nm line of a He–Ne laser as excitation source (LabRAM HR-Olympus Micro Raman system).

3. Results and discussion

Fig. 1 shows the typical SEM images of the as-grown doped and undoped ZnO nanostructures. As can be seen, the needle-like morphology of the undoped nanostructures does not change much on In doping. However, on Sb doping, the morphology changes initially to rod-like and then to particle-like nanostructures as the nominal Sb concentration increased. Incorporation of Ga results in the growth of nail-like structures with uniform diameter.

Fig. 2 shows the XRD patterns of the doped and undoped nanostructures. The XRD peaks of the undoped and doped samples match well with the wurtzite phase of ZnO [29]. Nevertheless, the XRD patterns of the as-grown In and Sb doped samples reveal some additional diffraction peaks that can not be related to wurtzite ZnO. Formation of $In(OH)_3$ and Sb_2O_3 as minority phases are responsible for such additional peaks as we reported earlier [26,27]. These minority phases can be successfully dissociated by thermal treatment at adequate conditions [26,27]. On the other hand, no additional diffraction peaks related to oxide or hydroxide phase of gallium are observed in as-grown Ga doped ZnO samples.

As can be observed from Fig. 2, indium doping leads to a decrease of the XRD peak intensity of the ZnO nanostructures. The effect is prominent for heavily doped (2.0%) sample, suggesting a loss of crystallinity of ZnO nanostructures due to indium incorporation. The difference of atomic radii between indium and zinc (1.66 and 1.38 Å respectively) probably is responsible for the distortion of ZnO lattice. The decrease of diffraction peak intensity is even more evident after thermal annealing due to an enhanced incorporation of indium into the ZnO nanostructures. Similar to indium doping, antimony doping results in the decrease of XRD peak intensity. However, the effect of doping is more prominent in the latter case.

Unlike In and Sb doping, Ga doping does not produce the formation of any minority phase, and hence no additional diffraction peak beside the wurtzite ZnO could be detected in their XRD patterns (Fig. 2). It is worth to note that instead of reducing the peak intensity, incorporation of gallium enhances the intensity of XRD peaks of ZnO. Since Ga and Zn have similar atomic radii (1.41 and 1.38 Å, respectively), no considerable lattice distortion is expected on Ga doping. Liang et al. [30] have reported the catalytic effect of Ga on the growth of ZnO nanostructures in chemical vapor deposition process. Catalytic effect of Ga might also be responsible for the better crystallinity of our Ga doped ZnO nanostructures.

Fig. 3 shows the variation of lattice parameters (a, c) of the as-grown and annealed ZnO nanostructures with the variation of dopant concentration. The refined values of a and c were estimated through the least squares procedure described by Giacovazzo et al. [31]. It can be noted that for as-grown samples, the lattice parameters are close to the reported bulk values of ZnO [32]. However, after thermal annealing, the lattice parameters of In and Sb doped samples deviate from the bulk values considerably. The effect is more prominent for the lattice parameter c of Sb doped samples, which suggests that incorporated Sb atoms occupy specific lattice sites, resulting in anisotropic distortion of the unit cell along the [001] direction. On the other hand, no significant variation of lattice parameters was observed on Ga doping, even after thermal annealing. Therefore, whereas incorporation of In and Sb causes considerable distortion of ZnO lattice, incorporation of Ga does not have any adverse effect on the lattice structure or crystallinity of ZnO nanostructures.

It is well known that vibrational properties of solids are related to the spatial array at long (space group) and short range orders (LVM's) of the constituent atoms. To study the effect of In, Sb, and Ga doping on the vibrational properties of ZnO nanostructures,

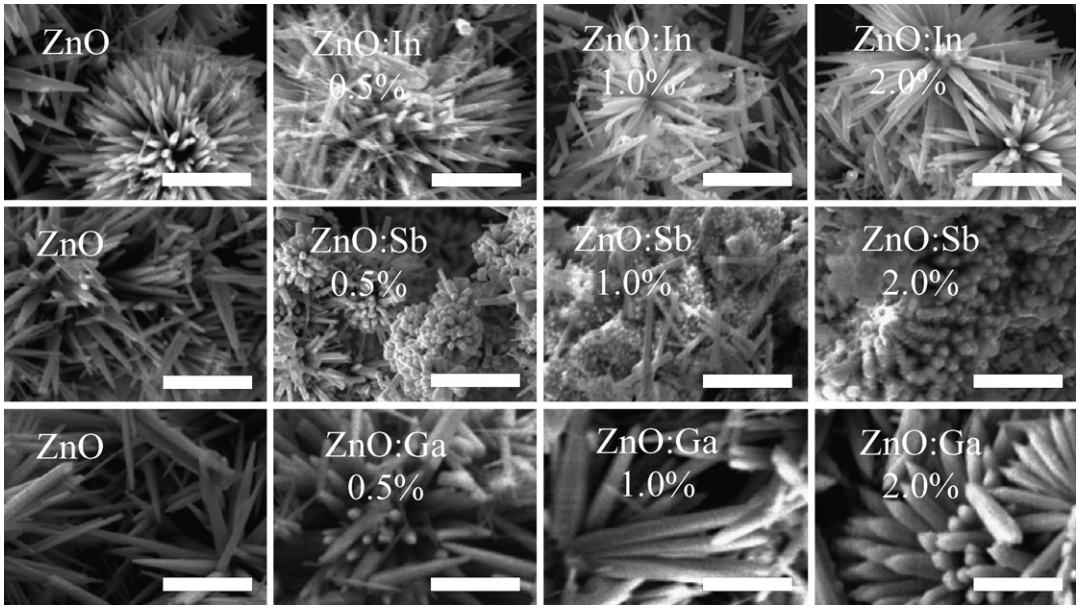

Fig. 1. Typical SEM images of the as-grown doped and undoped ZnO nanostructures. All the scale bars correspond to 5 μm.

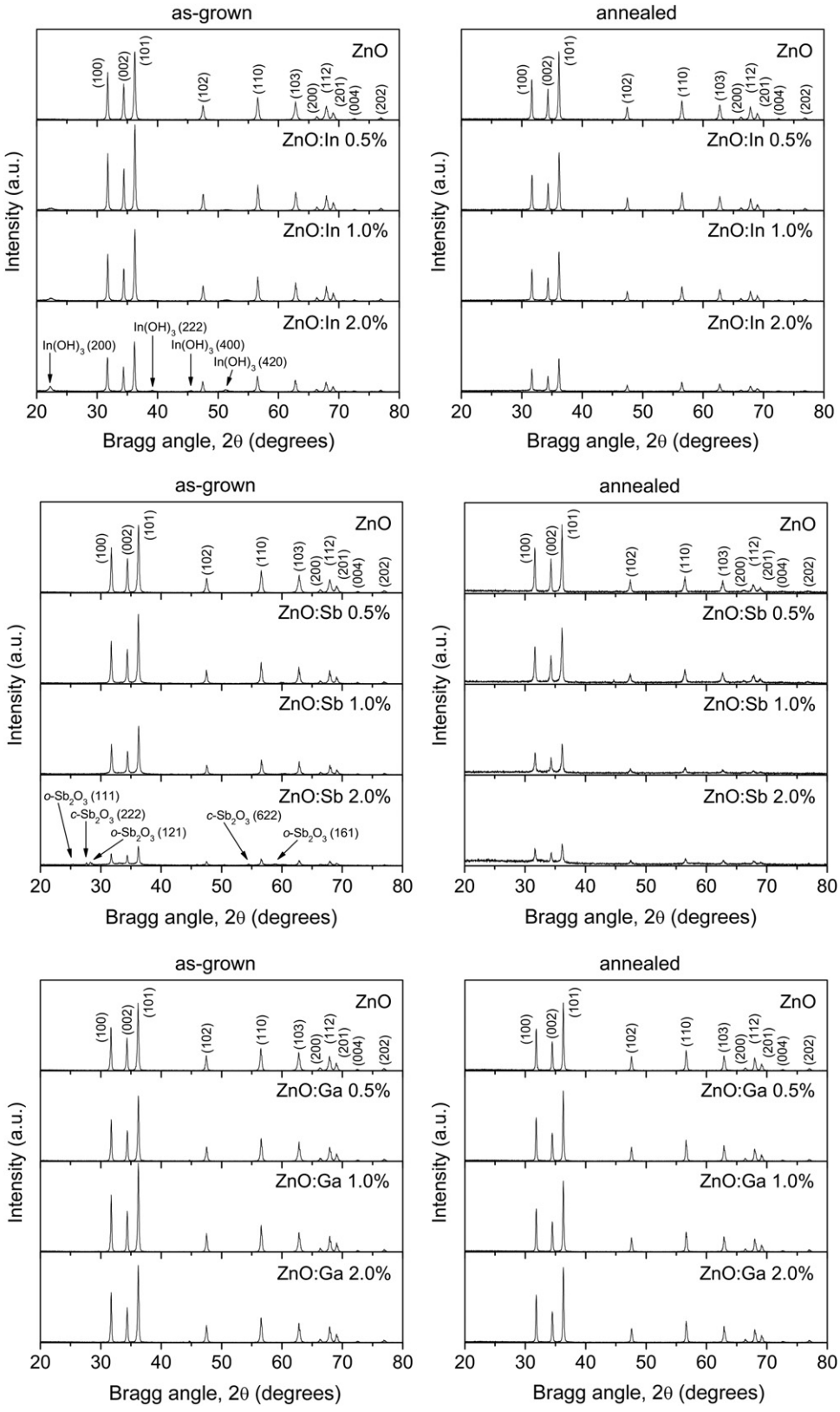

Fig. 2. XRD patterns of the as-grown and annealed ZnO nanostructures.

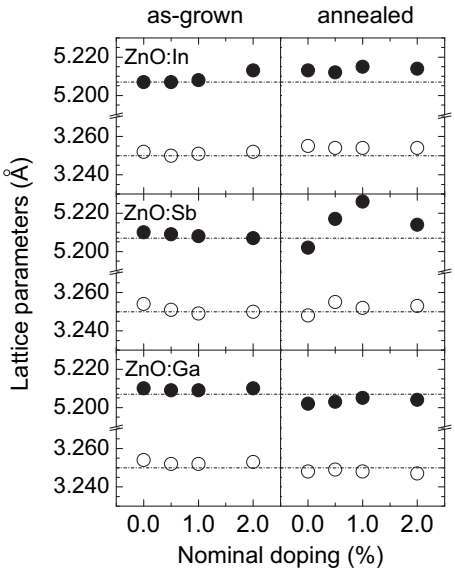

Fig. 3. Refined lattice parameters a (○) and c (●) of the doped and undoped ZnO nanostructures. The dotted lines correspond to lattice parameters reported by Heller et al. [32] for bulk ZnO ($a = 3.2495$ and $c = 5.2069$).

Raman spectroscopy was performed on the as-grown and annealed samples.

The symmetry of wurtzite ZnO lies in the spatial group C_{6v}^4, with two formula units in the primitive cell. Therefore, its optical phonons at the center of the Brillouin zone (Γ) can be represented by the following irreducible relation [33]:

$$\Gamma = 1A_1 + 2B_1 + 1E_1 + 2E_2, \quad (1)$$

A_1 and E_1 represent the two polar branches, which split into LO and TO components with different frequencies due to the macroscopic electric fields associated with the LO phonons. The two E_2 branches are nonpolar; while the low frequency mode (E_{2L}) is associated to the heavy Zn sub-lattice, the high frequency mode (E_{2H}) involves only the oxygen atoms [34]. All these A_1, E_1 and E_2 branches are Raman and infrared active. On the other hand, the two B_1 branches are both infrared and Raman inactive, and are so-called silent modes.

Table 1
Frequency and assignment of Raman peaks attributed to wurtzite ZnO observed in undoped as-grown and annealed samples.

Vibration frequency (cm^{-1})	Process
204	2-E_{2L} [22,36–38,46,47]; 2-TA (M) [38–41,47]
331	E_{2H}-E_{2L} [22,35,38,42,46,47]; 2-E_2 (M) [39,40,43]; TO-E_2^{41}
377	A_{1T} [19,35,40,41,44,46,47]
410	E_{1T} [19,35,40,41,44,46,47]
436	E_{2H} [19,35,40,41,44,46,47]
579	LO [16,35]
663	TA + LO [35,38,41,45,47]; $E_{2L} - B_{1H}$ [22]; $A_{1L} + E_{2L}$ [37]; 2-($E_{2H} - E_{2L}$) [38]

Fig. 4 shows the Raman spectra of the undoped and In doped samples, before and after thermal annealing process. The spectrum of the undoped and unannealed ZnO sample reveals seven peaks, located at about 204, 331, 377, 410, 436, 579 and 663 cm^{-1}. The peaks at 377, 410, 436 and 579 cm^{-1} are attributed to the A_{1T}, E_{1T}, E_{2H} and LO modes, respectively. The random orientation of ZnO nanocrystals produces the overlapping of the A_{1L} and E_{1L} modes, resulting in the single broad LO peak observed at around 579 cm^{-1} [35].

The peaks centered at about 204, 331, and 633 cm^{-1} have been previously observed in ZnO by several authors [22,35–43,45–47] and were attributed to the second order modes or multi-phonon processes. Positions and assignments of all the vibrational modes observed for the undoped as-grown and annealed samples attributed to first order, second order or multi-phonon process of wurtzite ZnO are summarized in Table 1.

The Raman spectra of as-grown indium doped samples revealed all the peaks we observed for undoped sample with an additional peak. The additional peak, located at about 312 cm^{-1}, can not be attributed to wurtzite ZnO or $In(OH)_3$. Jang et al. [41] have reported a Raman peak at about 316 cm^{-1} in their powder ZnO samples, and assigned it to a multi-phonon process involving a silent mode (LO-B_1). Manjón et al. [48] proposed that the breakdown of the translational crystal symmetry induced by defects and impurities allows the observation of silent modes. The frequencies of silent modes B_{1L} and B_{1H} in wurtzite ZnO were predicted at about 275 and 582 cm^{-1}, respectively [45]. Nevertheless, no Raman peaks at such frequencies are observed for our indium doped ZnO nanostructures.

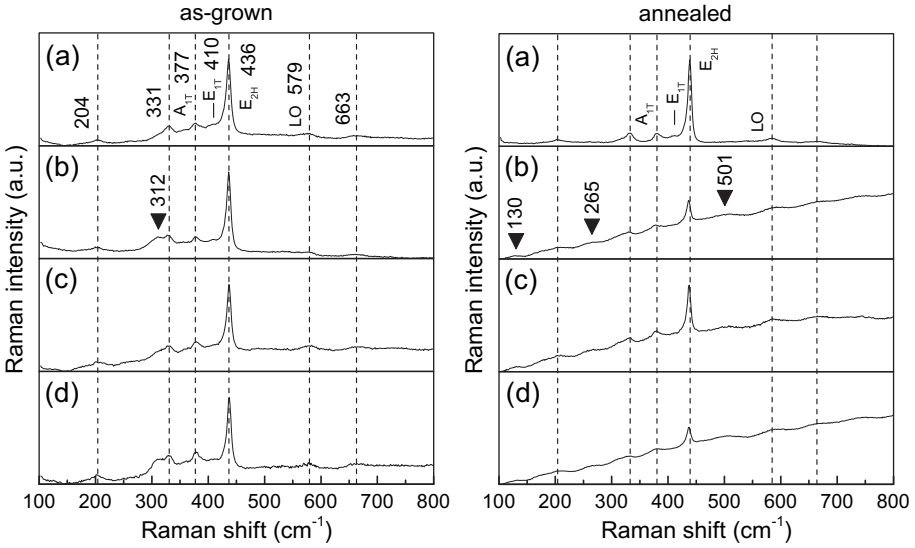

Fig. 4. Raman spectra of as-grown and annealed In doped ZnO nanostructures: a) undoped, b) 0.5%, c) 1.0%, and d) 2.0% nominal doping.

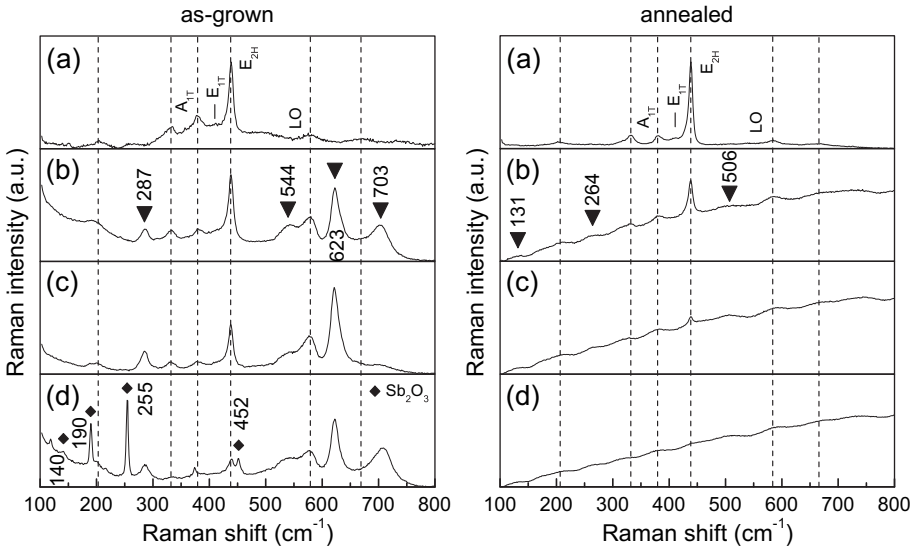

Fig. 5. Raman spectra of as-grown and annealed Sb doped ZnO nanostructures: a) undoped, b) 0.5%, c) 1.0%, and d) 2.0% nominal doping.

Therefore, we believe that the band observed at about 312 cm^{-1} does not involve a silent mode. To determine if the peak located at 312 cm^{-1} corresponds to an LVM due to substitutional indium (In_{Zn}) we estimated the frequency of such LVM using the effective masses (μ) relation [49], $\omega_{ZnO}/\omega_{LVM} \approx (\mu_{LVM}/\mu_{ZnO})^{1/2}$. However, as the estimated frequencies do not correspond to that of additional vibrational mode we observed for indium doped samples, it is feasible that the origin of 312 cm^{-1} Raman peak is not a point defect, like substitutional indium. We believe that a complex defect involving indium atoms is responsible for such anomalous mode observed in our indium doped ZnO samples.

On thermal annealing, in general, the intensity of the Raman peaks associated to wurtzite ZnO decreased as the nominal concentration of indium doping increased. This behavior can be attributed to the loss of crystallinity of the nanostructures due to indium incorporation as observed in their XRD patterns. Similar observations were made by Wang et al. [17] for their silver doped ZnO thin films. It is interesting to note that after thermal annealing, the peak located at about 312 cm^{-1} for the doped samples disappeared. Instead, three additional modes appeared at about 130, 265 and 501 cm^{-1}. The peaks at 265 and 501 can be attributed to the disorder activated Raman scattering of silent modes B_{1L} and 2-B_{2L} [48] respectively. The peak located at about 130 cm^{-1} has been already observed by Yadav et al. [46] in their Li- and Ni-doped ZnO samples, and attributed to zone boundary transverse acoustic mode at the critical point M [TA(M)]. As would be shown later, this vibrational mode appears also in our antimony and gallium doped samples. Therefore, it is feasible to assign this mode related to crystal ordering in the host lattice rather than the nature of doping element.

Fig. 5 shows the Raman spectra of antimony doped samples before and after thermal annealing. Undoped sample revealed seven Raman peaks, which could be attributed to first order, second order and multi-phonon process of wurtzite ZnO, as has been described earlier. In 0.5 and 1.0% (nominal) antimony doped samples, several broad peaks appear at about 287, 544, 623 and 703 cm^{-1}. However, none of them could be attributed to the LVM's due to the presence of SbZn point defects. For the sample with highest antimony doping (2.0% nominal), four additional sharp peaks centered at about 140, 190, 255 and 452 cm^{-1} appeared,

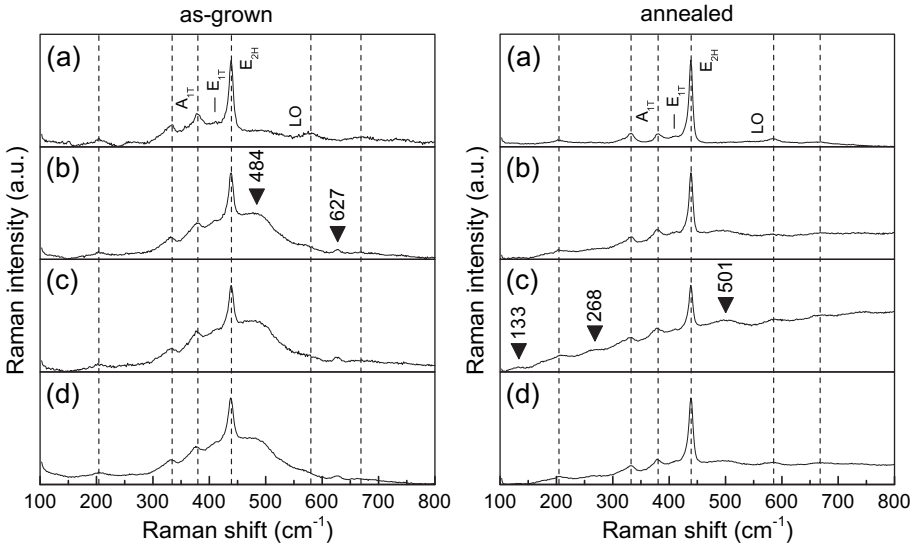

Fig. 6. Raman spectra of as-grown and annealed Ga doped ZnO nanostructures: a) undoped, b) 0.5%, c) 1.0%, and d) 2.0% nominal doping.

which could be attributed to the crystalline Sb_2O_3 [50] present as minority phase in the doped ZnO nanostructures. On thermal annealing, all those additional Raman peaks disappeared, confirming complete dissociation of Sb_2O_3, in agreement with observations made from their XRD spectra.

For as-grown samples, we can see a decrease of intensity of the Raman peaks associated to wurtzite ZnO with the increase of Sb content due to the loss of crystallinity of the nanostructures. After the annealing process, while the Raman peaks located at 287, 544, 623 and 703 cm^{-1} disappear, three new weak and broad bands appeared at about 131, 264, 506 cm^{-1}. The frequencies of these new bands match well with the bands observed in annealed indium doped samples, and attributed to the activation of vibrational frequencies involving a zone boundary phonon and two silent modes. It is worth to note that the decrease of the intensity of Raman peaks in thermally treated Sb doped samples is larger than the decrease we observed in indium doped samples. Furthermore, in the sample with highest Sb content, the E_{2H} peak of wurtzite ZnO is not easily discernible; suggesting a strong deformation of the host lattice, as we observed in the values of their lattice parameters (Fig. 2).

Fig. 6 shows the Raman spectra of Ga doped samples. There appeared a strong broad band centered at about 484 cm^{-1} and a weak band around 627 cm^{-1} for the as-grown samples. The positions of these bands do not match with the reported Raman peaks of Ga_2O_3 or other oxide phases of gallium [51]. On thermal annealing, these broad bands disappear and three weak bands located at 133, 268 and 501 cm^{-1} appear similar to the annealed indium and antimony doped samples.

Table 2 summarizes all the anomalous Raman bands observed for In, Sb and Ga doped ZnO nanostructures. It is worth to note that the frequency of observed anomalous modes remained fixed regardless of the doping concentration. On analyzing the Raman spectra of all the doped samples, it is observed that the Raman bands at about 130, 265 and 500 cm^{-1} appear in all the doped samples after thermal annealing. Therefore, the vibrational modes are not specific to the used dopants like In, Sb or Ga. It is reasonable to consider that these modes are the result of the breakdown of translational crystal symmetry induced by impurities, relaxing the selection rules for the phononic processes.

Among the most uncommon modes, the 312 cm^{-1} band appeared only for as-grown In doped samples is possibly due to a complex defect involving indium atoms. However, this complex defect must be immersed deep into the crystal environment, as it can not be observed in annealed samples with lower crystal quality. Same argument applies for the Raman bands at 287, 544 and 703 cm^{-1} for Sb doped samples, and 484 cm^{-1} for Ga doped samples.

Finally, the Raman band appeared at about 627 cm^{-1} in Ga doped samples, was also observed by Bundesmann et al. (631 cm^{-1}) [25]. They attributed it to a vibrational mode characteristic of gallium doped ZnO samples. Nevertheless, we observed a phonon mode at similar position (623 cm^{-1}) for as-grown Sb doped samples. We believe the mode is related to complex native defects rather than induced by incorporation of gallium in the ZnO nanostructures.

Table 2
Frequency of additional Raman peaks observed in as-grown and annealed In, Sb and Ga doped ZnO samples. Additional Raman peaks not related to silent or local vibrational mode are indicated in bold face.

Sample	Vibration frequency (cm^{-1})							
ZnO:In (as-grown)			**312**					
ZnO:In (annealed)	130	265			501			
ZnO:Sb (as-grown)			**287**			**544**	623	**703**
ZnO:Sb (annealed)	131	264			506			
ZnO:Ga (as-grown)				**484**			627	
ZnO:Ga (annealed)	133	268			501			

4. Conclusions

Effect of metal doping on the structure and vibrational modes of hydrothermally grown ZnO nanostructures has been studied systematically. While incorporation of In, and Sb induces lattice defects in the ZnO nanostructures, incorporation of Ga improves their crystalline quality due to catalytic effect. Incorporation of metals like In, Sb and Ga in ZnO nanostructures drastically modifies their vibrational properties, inducing the activation of silent modes, producing complex native defects, and induces some Raman active modes specific to the doping element.

Acknowledgements

The authors are thankful to M.C. Leticia Baños López for her help in taking XRD spectra. This work was partially supported by PROMEP-SEP (Grant No. PROMEP/103.5/09/4194) and VIEP-BUAP (Grant. PAU-EXC2010).

References

[1] S.Y. Lee, E.S. Shim, H.S. Kang, S.S. Pang, J.S. Kang, Fabrication of ZnO thin film diode using laser annealing, Thin Solid Films 473 (2005) 31–34.
[2] M.H. Huang, S. Mao, H. Feick, H. Yan, Y. Hu, H. Kind, E. Weber, R. Russo, P. Yang, Room-temperature ultraviolet nanowire nanolasers, Science 292 (2001) 1897–1899.
[3] Y.W. Zhu, H.Z. Zhang, X.C. Sun, S.Q. Feng, J. Xu, Q. Zhao, B. Xiang, R.M. Wang, D.P. Yu, Efficient field emission from ZnO nanoneedle arrays, Appl. Phys. Lett. 83 (2003) 144–146.
[4] Z. Fan, J.G. Lu, Gate-refreshable nanowire chemical sensors, Appl. Phys. Lett. 86 (2005) 123510 (3 pages).
[5] Y. Wang, M. Muhler, Ch. Wöll, Spectroscopic evidence for the partial dissociation of H_2O on ZnO(100), Phys. Chem. Chem. Phys. 8 (2006) 1521–1524.
[6] S.Y. Bae, C.W. Na, J.H. Kang, J. Park, Comparative structure and optical properties of Ga-, In-, and Sn-doped ZnO nanowires synthesized via thermal evaporation, J. Phys. Chem. B. 109 (2005) 2526–2531.
[7] F.-Q. He, Y.-P. Zhao, Growth of ZnO nanotetrapods with hexagonal crown, Appl. Phys. Lett. 88 (2006) 193113 (3 pages).
[8] J. Xiao, Y. Wu, X. Bai, W. Zhang, L. Tu, Controlled growth of ZnO pyramid arrays with nanorods and their field emission properties, J. Phys. D Appl. Phys. 41 (2008) 135409 (5 pages).
[9] U. Pal, P. Santiago, Controlling the morphology of ZnO nanostructures in a low-temperature hydrothermal process, J. Phys. Chem. B. 109 (2005) 15317–15321.
[10] H. Zhang, J. Wu, Ch. Zhai, N. Du, X. Ma, D. Yang, From ZnO nanorods to 3D hollow microhemispheres: solvothermal synthesis, photoluminescence and gas sensor properties, Nanotechnology 18 (2007) 455604 (7 pages).
[11] R. Wahab, S.G. Ansari, Y.S. Kim, M. Song, H.-Sh. Shin, The role of pH variation on the growth of zinc oxide nanostructures, Appl. Surf. Sci. 255 (2009) 4891–4896.
[12] L.J. Mandalapu, F.X. Xiu, Z. Yang, D.T. Zhao, J.L. Liu, *p*-type behavior from Sb-doped ZnO heterojunction photodiodes, Appl. Phys. Lett. 88 (2006) 112108 (3 pages).
[13] H. Wang, S. Baek, J. Song, J. Lee, S. Lim, Microstructural and optical characteristics of solution-grown Ga-doped ZnO nanorod arrays, Nanotechnology 19 (2008) 075607 (6 pages).
[14] J. Alaria, M. Venkatesan, J.M.D. Coey, Magnetism of ZnO nanoparticles doped with 3d cations prepared by a solvothermal method, J. Appl. Phys. 103 (2008) 07D123 (3 pages).
[15] J.U. Brehm, M. Winterer, H. Hahn, Synthesis and local structure of doped nanocrystalline zinc oxides, J. Appl. Phys. 100 (2006) 064311 (9 pages).
[16] C.L. Du, Z.B. Gu, Y.M. You, J. Kasim, T. Yu, Z.X. Shen, Z.H. Ni, Y. Ma, G.X. Cheng, Y.F. Chen, Resonant Raman spectroscopy of (Mn, Co)-codoped ZnO films, J. Appl. Phys. 103 (2008) 023521 (4 pages).
[17] X.B. Wang, C. Song, K.W. Geng, F. Zeng, F. Pan, Luminescence and Raman scattering properties of Ag-doped ZnO films, J. Phys. D Appl. Phys. 39 (2006) 4992–4996.
[18] J.B. Wang, H.M. Zhong, Z.F. Li, W. Lu, Raman study of N^+-implanted ZnO, Appl. Phys. Lett. 88 (2006) 101913 (3 pages).
[19] N. Hasuike, H. Fukumura, H. Harima, K. Kisoda, H. Matsui, H. Saeki, H. Tabata, Raman scattering studies on ZnO doped with Ga and N (codoping), and magnetic impurities, J. Phys. Condens. Matter 16 (2004) S5807–S5810.
[20] A. Kaschner, U. Haboeck, M. Strassburg, M. Strassburg, G. Kaczmarczyk, A. Hoffmann, C. Thomsen, A. Zeuner, H.R. Alves, D.M. Hofmann, B.K. Meyer,

Nitrogen-related local vibrational modes in ZnO:N, Appl. Phys. Lett. 80 (2002) 1909–1911.
[21] N.H. Nickel, K. Fleischer, Hydrogen local vibrational modes in zinc oxide, Phys. Rev. Lett. 90 (2003) 197402 (4 pages).
[22] J.D. Ye, S.L. Gu, S.M. Zhu, S.M. Liu, Y.D. Zheng, R. Zhang, Y. Shi, Q. Chen, H.Q. Yu, Y.D. Ye, Raman study of lattice dynamic behaviors in phosphorus-doped ZnO films, Appl. Phys. Lett. 88 (2006) 101905 (3 pages).
[23] M.-L. Tu, Y.-K. Su, C.-Y. Ma, Nitrogen-doped *p*-type ZnO films prepared from nitrogen gas radio-frequency magnetron sputtering, J. Appl. Phys. 100 (2006) 053705 (4 pages).
[24] F. Friedrich, N.H. Nickel, Resonant Raman scattering in hydrogen and nitrogen doped ZnO, Appl. Phys. Lett. 91 (2007) 111903 (3 pages).
[25] C. Bundesmann, N. Ashkenov, M. Schubert, D. Spemann, T. Butz, E.M. Kaidashev, M. Lorenz, M. Grundmann, Raman scattering in ZnO thin films doped with Fe, Sb, Al, Ga, and Li, Appl. Phys. Lett. 83 (2003) 1974–1976.
[26] A. Escobedo-Morales, M. Herrera-Zaldivar, U. Pal, Indium doping in nano-structured ZnO through low-temperature hydrothermal process, Opt. Mater. 29 (2006) 100–104.
[27] A. Escobedo-Morales, U. Pal, M. Herrera-Zaldivar, Incorporation of Sb in ZnO nanostructures through hydrothermal process, J. Nanosci. Nanotechnol. 8 (2008) 6551–6557.
[28] A. Escobedo-Morales, U. Pal, Defect annihilation and morphological improvement of hydrothermally grown ZnO nanorods by Ga doping, Appl. Phys. Lett. 93 (2008) 193120 (3 pages).
[29] JCPDS Card No. 36-1451.
[30] Y. Liang, X. Zhang, L. Qin, E. Zhang, H. Gao, Z. Zhang, Ga-assisted synthesis and optical properties of ZnO submicron- and nanotowers, J. Phys. Chem. B. 110 (2006) 21593–21595.
[31] C. Giacovazzo, H.L. Monaco, G. Artioli, D. Viterbo, G. Ferraris, G. Gilli, G. Zanotti, M. Catti, Fundamentals of Crystallography, International Union of Crystallography. Oxford Science Publications, USA, 2002.
[32] R.B. Heller, J. McGannon, A.H. Weber, Precision determination of the lattice constants of zinc oxide, J. Appl. Phys. 21 (1950) 1283–1284.
[33] C.A. Arguello, D.L. Rousseau, S.P.S. Porto, First-order Raman effect in wurtzite-type crystals, Phys. Rev. 181 (1969) 1351–1363.
[34] C.X. Xu, X.W. Sun, X.H. Zhang, L. Ke, S.J. Chua, Photoluminescent properties of copper-doped zinc oxide nanowires, Nanotechnology 15 (2004) 856–861.
[35] Th.-L. Phan, R. Vincent, D. Cherns, N.H. Dan, S.-Ch. Yu, Enhancement of multiple-phonon resonant Raman scattering in Co-doped ZnO nanorods, Appl. Phys. Lett. 93 (2008) 082110 (3 pages).
[36] H.W. Kunert, D.J. Brink, F.D. Auret, J. Malherbe, J. Barnas, V. Kononenko, Multiphonon processes in ZnO, Phys. Stat. Sol. C 2 (2005) 1131–1136.
[37] Z.X. Cheng, X.L. Wang, S.X. Dou, K. Ozawa, H. Kimura, P. Munroe, Fabrication, Raman spectra and ferromagnetic properties of the transition metal doped ZnO nanocrystals, J. Phys. D Appl. Phys. 40 (2007) 6518–6521.
[38] X. Wang, J. Xu, X. Yu, K. Xue, J. Yu, X. Zhao, Structural evidence of secondary phase segregation from the Raman vibrational modes in $Zn_{1-x}Co_xO$ ($0 < x < 0.6$), Appl. Phys. Lett. 91 (2007) 031908 (3 pages).
[39] M. Rajalakshmi, A.K. Arora, B.S. Bendre, S. Mahamuni, Optical phonon confinement in zinc oxide nanoparticles, J. Appl. Phys. 87 (2000) 2445–2448.
[40] L.W. Yang, X.L. Xu, G.S. Huang, T. Qiu, Y.M. Yang, In situ synthesis of Mn-doped ZnO multileg nanostructures and Mn-related Raman vibration, J. Appl. Phys. 97 (2005) 014308 (4 pages).
[41] M.S. Jang, M.K. Ryu, M.H. Yoon, S.H. Lee, H.K. Kim, A. Onodera, S. Kojima, A study on the Raman spectra of Al-doped and Ga-doped ZnO ceramics, Curr. Appl. Phys. 9 (2009) 651–657.
[42] C. Xu, M. Kim, J. Chun, D. Kim, Growth of Ga-doped ZnO nanowires by two-step vapor phase method, Appl. Phys. Lett. 86 (2005) 133107 (3 pages).
[43] H.K. Yadav, K. Sreenivas, R.S. Katiyar, V. Gupta, Defect induced activation of Raman silent modes in RF co-sputtered Mn doped ZnO thin films, J. Phys. D Appl. Phys. 40 (2007) 6005–6009.
[44] T.D. Damen, S.P.S. Porto, B. Tell, Raman effect in zinc oxide, Phys. Rev. 142 (1966) 570–574.
[45] J. Serrano, A.H. Romero, F.J. Manjón, R. Lauck, M. Cardona, A. Rubio, Pressure dependence of the lattice dynamics of ZnO: an ab initio approach, Phys. Rev. B. 69 (2004) 094306 (14 pages).
[46] (a) H.K. Yadav, K. Sreenivas, V. Gupta, R.S. Katiyar, Low-frequency zone boundary phonons in Li doped ZnO ceramics, J. Appl. Phys. 104 (2008) 053507 (5 pages);
(b) H.K. Yadav, K. Sreenivas, V. Gupta, R.S. Katiyar, Structural studies and Raman spectroscopy of forbidden zone boundary phonons in Ni-doped ZnO ceramics, J. Raman Spectrosc. 40 (2009) 381–386.
[47] R. Cuscó, E. Alarcón-Lladó, J. Ibáñez, L. Artús, J. Jiménez, B. Wang, M.J. Callahan, Temperature dependence of Raman scattering in ZnO, Phys. Rev. B. 75 (2007) 165202 (11 pages).
[48] F.J. Manjón, B. Marí, J. Serrano, A.H. Romero, Silent Raman modes in zinc oxide and related nitrides, J. Appl. Phys. 97 (2005) 053516 (4 pages).
[49] A. Kaschner, H. Siegle, G. Kaczmarczyk, M. Straßburg, A. Hoffmann, C. Thomsen, U. Birkle, S. Einfeldt, D. Hommel, Local vibrational modes in Mg-doped GaN grown by molecular beam epitaxy, Appl. Phys. Lett. 74 (1999) 3281–3283.
[50] C.A. Cody, L. DiCarlo, R.L. Darlington, Vibrational and thermal study of antimony oxides, Inorg. Chem. 18 (1979) 1572–1576.
[51] H.J. Chun, Y.S. Choi, S.Y. Bae, H.W. Seo, S.J. Hong, J. Park, H. Yang, Controlled structure of gallium oxide nanowires, J. Phys. Chem. B. 107 (2003) 9042–9046.